Nanostructures

DOI: 10.1002/anie.201402709

Photocatalytic Au–Bi_2S_3 Heteronanostructures**

*Goutam Manna, Riya Bose, and Narayan Pradhan**

Abstract: *Au–Bi_2S_3 heteronanostructure photocatalysts were designed in which the coupling of a metal plasmon and a semiconductor exciton aids the absorption of solar light, enhances charge separation, and results in improved catalytic activity. Furthermore, these nanostructures show a unique pattern of structural combination, with Au nanoparticles positioned at the center of Bi_2S_3 nanorods. The chemistry of formation of these nanostructures, their epitaxy at the junction, and their photoconductance were studied, as well as their photoresponse properties.*

The design of new functional materials with useful materials properties required for various technological applications has remained in forefront research for decades.[1–10] Among these, heterostructured nanomaterials having noble metal and semiconductor junctions are categorized as one of the leading materials.[3,11–17] Apart from having the individual properties of both of the constituents, here, the interaction between quantum confined electronic states of semiconductor and dielectric confined electronic modes in the metal domain, leads to the generation of new optoelectronic properties.[18–21] The plasmon-induced electric field enhances the absorption cross-section of the semiconductor domain and can strongly affect the exciton dynamics.[3,16,22,23] Mixing of electronic states at the metal–semiconductor interface also facilitates intraparticle charge transfer.[3,10,11,13,24] Both effects make these materials suitable for the harvesting of solar light and its transformation into chemical/electrical energy, and hence for implementation in photocatalysis, photovoltaics, optoelectronics, biological labeling, and other areas.[13,14,25–27] The noble metals Au and Ag coupled with TiO_2, ZnO, CdSe, CdS, and PbS have been widely used for such applications.[13,26–31] Literature study revealed that these materials broadly follow two types of carrier-transformation pathways on visible-light irradiation. In one case, the hot electron generated from the surface plasmon of the noble metal is transferred to the semiconductor, and in the other case, the photogenerated electron moves from the semiconductor to metal. The second case is normally observed when the semiconductor absorbs the visible light and has the advantage that more solar light is harvested, as the absorption bands of both entities remain in the visible window. However, most of such systems are limited to cadmium- and lead-based semiconductor heterostructures, the toxicity of which remains a major concern. For the effective implementation of these heterostructures, research is continuing in the search for less- or nontoxic systems in which both the components can absorb visible or near-IR light and show effective interference of their electronic states for efficient carrier transportation.

Unfortunately, the random synthesis of such metal–semiconductor heteronanostructures faces several practical difficulties. For efficient carrier mobility in the heterostructures, a strong exciton–plasmon coupling is required. Such type of coupling is only possible if an epitaxial connection between the metal and the semiconductor is established at their interface; however, the difference in the lattice parameters of the two materials mostly restricts epitaxy formation. Hence, the development of new materials is required for effective carrier transformation and show desirable properties.

Herein we describe the development of a new heterostructured nanomaterial comprising Bi_2S_3 and Au. These materials have approximately 2–3% lattice mismatch (see Table S1 in the Supporting Information). Moreover, Bi_2S_3 is a low-bandgap (1.3 eV) semiconductor with a high absorption coefficient, which makes it an efficient absorber of solar light; it has already been widely implemented in photovoltaics.[32] In our study, a unique synthetic mechanism enabled controlled 1D agglomeration of Bi_2S_3 0D nanocrystals on Au particles. This process led to the formation of heterostructures with Au at the center of Bi_2S_3 1D nanorods. A clear epitaxial connection between the two counterparts was observed. The resulting material was a different kind of metal–semiconductor heterostructure to those previously synthesized, and its synthesis differs from the established mechanism of formation of heteronanostructures. In previously reported structures, Au was typically located at the tips of the rods; in our case, intriguingly, Au is located at the center. These structures also serve as ideal photocatalysts for dye reduction and show improved photoconductance and photoresponse. Herein we report the synthesis, structural characterization, photocatalysis, and photoresponse properties of these heterostructures.

In a typical reaction, the Au–Bi_2S_3 heteronanostructures were synthesized from $Bi(OAc)_3$ (origin of Bi), hexamethyldisilathiane (HMS; origin of S), $HAuCl_4$ (origin of Au), and a mixture of oleic acid and oleylamine as the solvent/capping agent. The solution of HMS in 1-octadecene (ODE) and the solution of $HAuCl_4$ in oleylamine were injected into the reaction flask containing $Bi(OAc)_3$ in oleic acid at about 170 °C. Bright- and dark-field microscopic images of the heteronanostructures showed that Au was placed at the center of the Bi_2S_3 nanorods (Figure 1).

[*] G. Manna, R. Bose, Dr. N. Pradhan
Department of Materials Science and Centre for Advanced Materials
Indian Association for the Cultivation of Science
Kolkata 700032 (India)
E-mail: camnp@iacs.res.in
Homepage: http://iacs.res.in/matsc/msnp/

[**] The DST Swarnajayanti (DST/SJF/CSA-01/2010-2012) project is acknowledged for funding. The research group of Prof. A. K. Nandi is acknowledged for helping with the photocurrent measurements.

Supporting information for this article is available on the WWW under http://dx.doi.org/10.1002/anie.201402709.

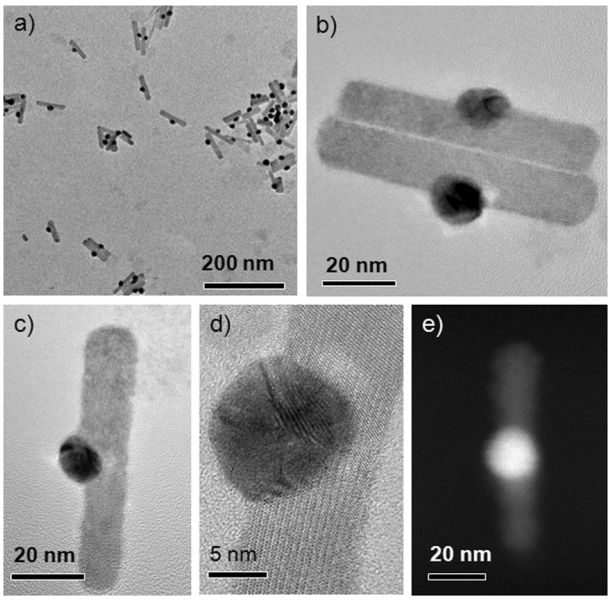

Figure 1. a–d) Transmission electron microscopy (TEM) image of Au–Bi_2S_3 heterostructures at different resolutions. e) High-angle annular dark-field scanning transmission electron microscopy (HAADF-STEM) image of a single heteronanorod.

By powdered X-ray diffraction (Figure 2a), the crystal phase of Bi_2S_3 was identified as orthorhombic with the space group *Pbnm*(62) (ICSD # 89324), and that of Au was found to be cubic. A high-resolution transmission electron microscopic image showed that the rods had grown along the [001] direction. From the *d* spacing of Au and Bi_2S_3, it was further observed that the epitaxy was formed between (101) planes of Au and (221) planes of Bi_2S_3 (Figure 2b). Figure 2c shows an atomic model of the heterostructure.

As the location of Au nanoparticles at the center of semiconductor nanorods is rare and unique among gold–semiconductor heterostructures, we investigated the formation mechanism of such structures by studying the intermediate samples obtained after the addition of the Au and S precursors to the reaction mixture at 170 °C. TEM images of the intermediate products clearly indicated that Bi_2S_3 particles with a size of approximately 3 nm were formed initially in the reaction medium, and then oriented in a regular way to form the nanorods (see Figure S1 in the Supporting Information). Even when a control reaction was performed without the addition of Au, Bi_2S_3 rod formation by a similar oriented-attachment process was observed. However, in the presence of Au nanoparticles, which were formed immediately after injection of the solution of the Au precursor in oleylamine, rod formation with Au nanoparticles at the center was facilitated, and importantly, it was observed to be much (ca. 3 times) faster than the control reaction. This result suggests that Au particles catalyze and enhance the rate of the 1D agglomeration of the Bi_2S_3 nanoparticles. In the presence of gold, Bi_2S_3 nanoparticles agglomerate along the [001] direction, which has minimized lattice mismatch with gold (ca. 2.81 %; Figure 2b; see Figure S2 for a schematic representation of the agglomeration of Bi_2S_3 in the presence of Au). A similar metal-catalyzed agglomeration process of nanoparticles was observed previously for ZnO nanorods.[33,34] However, an increase in the reaction temperature can enable agglomeration around the entire periphery of the Au particles, thus leading to the formation of core/shell nanostructures (see Figure S3).

The most important feature of these heterostructures is the optical-absorption window. Figure 3 shows the absorption spectra of Au, Bi_2S_3, and the Au–Bi_2S_3 heterostructures. The surface plasmon resonance (SPR) peak (at ca. 520 nm), which is the typical characteristic of gold nanoparticles, is broadened and redshifted (to ca. 560 nm) in the case of the heterostructures. This phenomenon is well-known for gold–semiconductor heterostructures, in which exciton–plasmon coupling and the high dielectric constant of the semiconductor cause the broadening and redshifting of the metal plasmonic peak.[3,22,35]

To utilize this exciton–plasmon coupling in the heterostructures, we further explored them as visible-light photocatalysts for dye reduction. Methylene blue (MB), which has a distinct absorption peak at approximately 660 nm, was chosen as the model dye. Upon reduction by two electrons, it forms leucomethylene blue (LMB), which is colorless; hence, the change is visible to the naked eye.[13] The reduction was established from the change in the nature of the absorption spectra (see Figure S4 for the details of this process). It was carried out with monochromatic light of wavelength 500 nm, at which the absorption of the dye is minimum (see Figure S5 for the time-dependent reduction of methylene blue). To demonstrate the superiority of the heterostructures, we carried out similar dye reduction in the presence of separate Au and Bi_2S_3 nanoparticles and with a mixture of Au and Bi_2S_3. We found that after 40 min, 10 and 14 % of the dye had been reduced by separate Au and Bi_2S_3 nanoparticles, respectively. Even a mixture of Au and Bi_2S_3 nanoparticles was able to reduce only

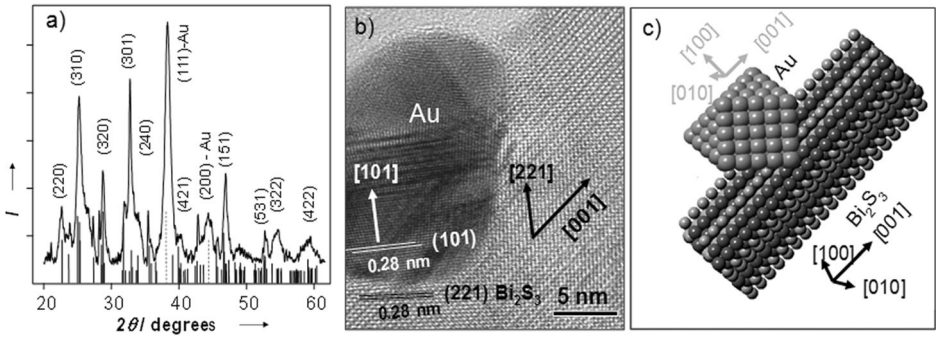

Figure 2. a) XRD pattern of the Au–Bi_2S_3 heteronanostructures. Solid vertical lines at the bottom indicate the XRD peak positions of bulk Bi_2S_3, and dotted lines correspond to cubic Au. b) High-resolution transmission electron microscopy (HRTEM) image of a heterojunction with labeled planes. c) Atomic model of a typical Au–Bi_2S_3 heterostructure.

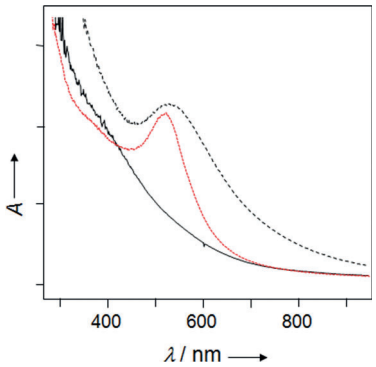

Figure 3. Absorption spectra of Au particles (dotted line), Bi_2S_3 rods (solid line), and Au–Bi_2S_3 heterostructures (dashed line).

about 28% of the dye, whereas with the heterostructures, about 80% of the dye was reduced under similar reaction conditions. We also measured the reduction rates for each individual process. The photoreduction of MB follows first-order kinetics expressed by $\ln(C_o/C) = Kt$, in which C_o is the concentration of MB at the adsorption equilibrium, and C is the residual concentration after different time intervals of illumination. These calculations again showed that the rate was fastest for the heterostructures (Figure 4c). A schematic representation of the photocatalytic dye-reduction process is shown in Figure 4a. Not only methylene blue, but also other dyes, such as rhodamine B, rhodamine 6G, and fuchsine, changed their colors very rapidly, which clearly proved the photocatalytic efficiency of the heterostructures. After one cycle of the reduction, we also examined the TEM images of the nanostructures, which were observed to be almost unchanged (see Figure S6). However, we could not transfer the nanostructures to water through thiolate ligand exchange, as thiols were found to etch Bi as well as Au from the nanostructures, and hence the reduction was carried out in a biphasic process in which the dye was kept in aqueous medium.

To understand the mechanism of dye reduction by these heterostructures, we studied the relative band alignment of Au and Bi_2S_3. According to previous reports, the Fermi level of Au is more positive (0.5 V versus the normal hydrogen electrode, NHE) than the conduction band of Bi_2S_3 (0.108 V versus NHE; Figure 4b).[3,36] We expect that the exciton–plasmon coupling further helps to equilibrate the Fermi level, and hence charge transfer from Bi_2S_3 to the Au nanoparticles became thermodynamically favorable. This coupling behaves typically like a metal–semiconductor heterojunction, whereby the photogenerated electron of the semiconductor is transferred effectively to the metal. This transfer enhances the reduction efficiency of the heterostructures. A previous study further revealed that the reduction of the dye on the Au surface occurs in presence of an electron donor, such as $NaBH_4$, which injects the electron into the gold to trigger the dye reduction.[37] Similarly, in our case, it is expected that the electron from the semiconductor is transferred to Au, which then promotes the reduction. A similar electron-transfer mechanism was proposed previously for Au–CdSe.[13]

Apart from photoreduction, these heterostructures also show enhanced photoconductance as compared to that of Bi_2S_3-only nanostructures. This result again supports improved charge separation in the heterostructures. Figure 5a shows the current–voltage plot of these heterostructures in the dark and under irradiation with white light; the equivalent plot for Bi_2S_3 alone is shown in the inset. For these measurements (see the Supporting Information for the detailed experimental procedure), a thin film of the nanocrystals was made by spin casting a solution of the nanocrystals in toluene on a glass substrate, and Au electrodes were deposited on the resulting film. Although both of these nanostructures showed enhancement of the current flow under illumination, Au–Bi_2S_3 showed higher photoconductance. Upon irradiation at 100 mW with white light, the photocurrent increased to approximately 1.7×10^{-5} A at a bias voltage of 4 V, whereas for Bi_2S_3 it remained only 1.9×10^{-8} A under similar conditions. This improvement in photoconductivity occurs because of efficient charge separation in the heterostructures as a result of suitable band alignment of Au and Bi_2S_3 and their coupling. We also measured the photoresponse of these heterostructures by periodically turning on and off the white

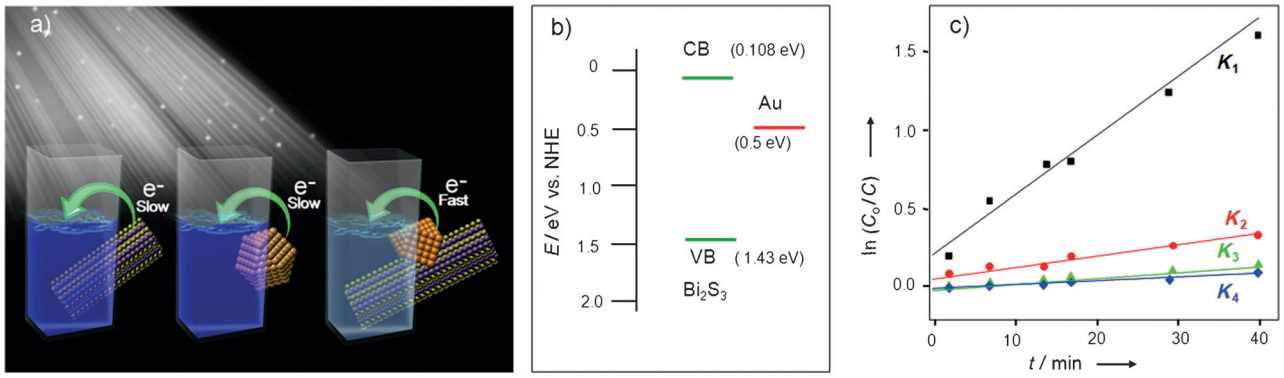

Figure 4. a) Schematic representation of conditions for the favorable photoreduction of methylene blue. b) Band alignment of Bi_2S_3 and Au (CB = conduction band, VB = valence band). c) Rate of dye degradation with irradiation progress under different conditions. The samples were irradiated using Xe lamp with a wavelength of 500 nm. K_1 (0.037 min^{-1}), K_2 (0.007 min^{-1}), K_3 (0.004 min^{-1}), and K_4 (0.002 min^{-1}) are the dye-degradation rate constants with Au–Bi_2S_3, a mixture of Au and Bi_2S_3, Bi_2S_3, and Au, respectively. For representative absorption spectra showing the change in the optical density of the dye during the reduction, see Figure S4 in the Supporting Information.

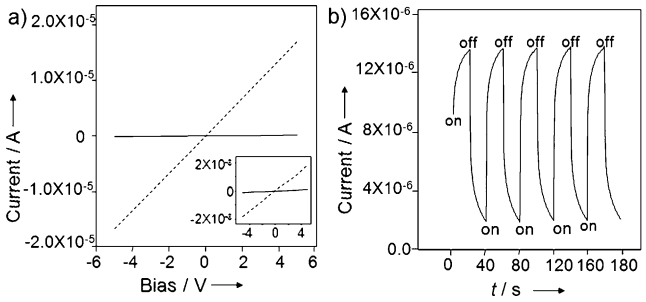

Figure 5. a) *I–V* characteristics of the Au–Bi_2S_3 heterostructure in the dark (solid line) and under illumination with white light from a Xe lamp with an intensity of 100 mW cm^2 and a bias voltage of 4 V (dotted line). The equivalent relationships for Bi_2S_3 are shown in the inset. b) Photoresponse characteristics of Au–Bi_2S_3 under illumination with white light. After as many as five cycles, the behavior of the heterostructures remained unchanged.

light (Figure 5b). Considerably high photosensitivity was observed: The current increased from 1.5×10^{-6} to 14.5×10^{-6} A in response to the on-and-off operation for a duration of 20 s. Even after a number of cycles, the photocurrent could still be changed by illumination switching; thus, the constructed device was fairly stable and reversible.

In conclusion, we have reported herein a new heterostructure Au–Bi_2S_3, in which both constituent materials show absorption within the solar spectrum. The intriguing pattern of Au present at the center of the rods rather than at the tips, as reported traditionally. This structure behaves as a typical metal–semiconductor Schottky junction, whereby the photogenerated electrons migrate from the semiconductor to the metal, thus leading to improved hole–electron separation. In turn, this behavior enhances the efficiency of the catalytic, photocurrent, and photoresponse properties of these materials. We believe that the design of such materials is timely and will be useful for various applications.

Received: February 24, 2014
Revised: April 7, 2014
Published online: May 20, 2014

Keywords: bismuth · gold · electron transfer · heterostructures · photocatalysts

[1] G. Manna, R. Bose, N. Pradhan, *Angew. Chem.* **2013**, *125*, 6894 – 6898; *Angew. Chem. Int. Ed.* **2013**, *52*, 6762 – 6766.
[2] D. Mocatta, G. Cohen, J. Schattner, O. Millo, E. Rabani, U. Banin, *Science* **2011**, *332*, 77 – 81.
[3] J.-S. Lee, E. V. Shevchenko, D. V. Talapin, *J. Am. Chem. Soc.* **2008**, *130*, 9673 – 9675.
[4] Y. Yin, R. M. Rioux, C. K. Erdonmez, S. Hughes, G. A. Somorjai, A. P. Alivisatos, *Science* **2004**, *304*, 711 – 714.
[5] N. Pradhan, D. Goorskey, J. Thessing, X. Peng, *J. Am. Chem. Soc.* **2005**, *127*, 17586 – 17587.
[6] A. Sahu, M. S. Kang, A. Kompch, C. Notthoff, A. W. Wills, D. Deng, M. Winterer, C. D. Frisbie, D. J. Norris, *Nano Lett.* **2012**, *12*, 2587 – 2594.
[7] V. A. Vlaskin, N. Janssen, J. van Rijssel, R. Beaulac, D. R. Gamelin, *Nano Lett.* **2010**, *10*, 3670 – 3674.
[8] P. K. Santra, P. V. Kamat, *J. Am. Chem. Soc.* **2012**, *134*, 2508 – 2511.
[9] K. Kravchyk, L. Protesescu, M. I. Bodnarchuk, F. Krumeich, M. Yarema, M. Walter, C. Guntlin, M. V. Kovalenko, *J. Am. Chem. Soc.* **2013**, *135*, 4199 – 4202.
[10] M. Jakob, H. Levanon, P. V. Kamat, *Nano Lett.* **2003**, *3*, 353 – 358.
[11] K. K. Haldar, G. Sinha, J. Lahtinen, A. Patra, *ACS Appl. Mater. Interfaces* **2012**, *4*, 6266 – 6272.
[12] T. Mokari, E. Rothenberg, I. Popov, R. Costi, U. Banin, *Science* **2004**, *304*, 1787 – 1790.
[13] R. Costi, A. E. Saunders, E. Elmalem, A. Salant, U. Banin, *Nano Lett.* **2008**, *8*, 637 – 641.
[14] E. Elmalem, A. E. Saunders, R. Costi, A. Salant, U. Banin, *Adv. Mater.* **2008**, *20*, 4312 – 4317.
[15] R. de Paiva, R. Di Felice, *ACS Nano* **2008**, *2*, 2225 – 2236.
[16] E. Khon, A. Mereshchenko, A. N. Tarnovsky, K. Acharya, A. Klinkova, N. N. Hewa-Kasakarage, I. Nemitz, M. Zamkov, *Nano Lett.* **2011**, *11*, 1792 – 1799.
[17] N. Zhao, J. Vickery, G. Guerin, J. I. Park, M. A. Winnik, E. Kumacheva, *Angew. Chem.* **2011**, *123*, 4702 – 4706; *Angew. Chem. Int. Ed.* **2011**, *50*, 4606 – 4610.
[18] A. Figuerola, M. van Huis, M. Zanella, A. Genovese, S. Marras, A. Falqui, H. W. Zandbergen, R. Cingolani, L. Manna, *Nano Lett.* **2010**, *10*, 3028 – 3036.
[19] M.-C. Daniel, D. Astruc, *Chem. Rev.* **2004**, *104*, 293 – 346.
[20] A. Vaneski, A. S. Susha, J. Rodríguez-Fernández, M. Berr, F. Jäckel, J. Feldmann, A. L. Rogach, *Adv. Funct. Mater.* **2011**, *21*, 1547 – 1556.
[21] I. A. Larkin, M. I. Stockman, M. Achermann, V. I. Klimov, *Phys. Rev. B* **2004**, *69*, 121403.
[22] E. Shaviv, O. Schubert, M. Alves-Santos, G. Goldoni, R. Di Felice, F. Vallée, N. Del Fatti, U. Banin, C. Sönnichsen, *ACS Nano* **2011**, *5*, 4712 – 4719.
[23] G. Sagarzazu, K. Inoue, M. Saruyama, M. Sakamoto, T. Teranishi, S. Masuo, N. Tamai, *Phys. Chem. Chem. Phys.* **2013**, *15*, 2141 – 2152.
[24] R. Costi, G. Cohen, A. Salant, E. Rabani, U. Banin, *Nano Lett.* **2009**, *9*, 2031 – 2039.
[25] X. Liu, C. Lee, W.-C. Law, D. Zhu, M. Liu, M. Jeon, J. Kim, P. N. Prasad, C. Kim, M. T. Swihart, *Nano Lett.* **2013**, *13*, 4333 – 4339.
[26] T.-T. Yang, W.-T. Chen, Y.-J. Hsu, K.-H. Wei, T.-Y. Lin, T.-W. Lin, *J. Phys. Chem. C* **2010**, *114*, 11414 – 11420.
[27] R. Debnath, M. T. Greiner, I. J. Kramer, A. Fischer, J. Tang, D. A. R. Barkhouse, X. Wang, L. Levina, Z.-H. Lu, E. H. Sargent, *Appl. Phys. Lett.* **2010**, *97*, 023109/1.
[28] H. Tada, T. Mitsui, T. Kiyonaga, T. Akita, K. Tanaka, *Nat. Mater.* **2006**, *5*, 782 – 786.
[29] M. Murdoch, G. I. N. Waterhouse, M. A. Nadeem, J. B. Metson, M. A. Keane, R. F. Howe, J. Llorca, H. Idriss, *Nat. Chem.* **2011**, *3*, 489 – 492.
[30] T. Wang, Z. Jiao, T. Chen, Y. Li, W. Ren, S. Lin, G. Lu, J. Ye, Y. Bi, *Nanoscale* **2013**, *5*, 7552 – 7557.
[31] D. V. Talapin, J.-S. Lee, M. V. Kovalenko, E. V. Shevchenko, *Chem. Rev.* **2010**, *110*, 389 – 458.
[32] G. Konstantatos, L. Levina, J. Tang, E. H. Sargent, *Nano Lett.* **2008**, *8*, 4002 – 4006.
[33] C. Pacholski, A. Kornowski, H. Weller, *Angew. Chem.* **2002**, *114*, 1234 – 1237; *Angew. Chem. Int. Ed.* **2002**, *41*, 1188 – 1191.
[34] K. M. AbouZeid, M. B. Mohamed, M. S. El-Shall, *Small* **2011**, *7*, 3299 – 3307.
[35] D. Mongin, E. Shaviv, P. Maioli, A. Crut, U. Banin, N. Del Fatti, F. Vallée, *ACS Nano* **2012**, *6*, 7034 – 7043.
[36] Z. Fang, Y. Liu, Y. Fan, Y. Ni, X. Wei, K. Tang, J. Shen, Y. Chen, *J. Phys. Chem. C* **2011**, *115*, 13968 – 13976.
[37] T. K. Sau, A. Pal, T. Pal, *J. Phys. Chem. B* **2001**, *105*, 9266 – 9272.

